Excitability and oscillations of active droplets

Ivar S. Haugerud, Hidde D. Vuijk, Job Boekhoven, Christoph A. Weber

Angaben zur Veröffentlichung / Publication details:

Haugerud, Ivar S., Hidde D. Vuijk, Job Boekhoven, and Christoph A. Weber. 2026. "Excitability and oscillations of active droplets." *Physical Review Letters* 136 (21): 218401. https://doi.org/10.1103/g9dh-ymx9.

Excitability and Oscillations of Active Droplets

Ivar S. Haugerud,[1] Hidde D. Vuijk,[1] Job Boekhoven,[2] and Christoph A. Weber[1,*]
[1]Faculty of Mathematics, Natural Sciences, and Materials Engineering: Institute of Physics, University of Augsburg, Universitätsstraße 1, 86159 Augsburg, Germany
[2]School of Natural Sciences, Department of Bioscience, Technical University of Munich, Lichtenbergstraße 4, 85748 Garching, Germany

(Received 28 April 2025; revised 4 November 2025; accepted 31 March 2026; published 27 May 2026)

In the field of biomolecular condensates and synthetic systems, it is an open question whether liquid droplets can undergo self-sustained oscillations of formation and dissolution. To unravel the minimal physicochemical prerequisite for such droplet oscillations, we present a simple model composed of only two independent chemical components with their diffusive and chemical fluxes governed by nonequilibrium thermodynamics. There is turnover of fuel that maintains a chemical reaction away from equilibrium, leading to active droplets. We find that a single active droplet undergoes a saddle-node bifurcation in the droplet volume upon increasing the fueling strength. Strikingly, the active droplet becomes excitable upon adding a further chemical reaction. For sufficient fueling, the system undergoes self-sustained oscillations.

DOI: 10.1103/g9dh-ymx9

Introduction—Oscillations of concentrations are relevant to numerous biological processes, including the circadian rhythm [1,2] and the cell cycle [3,4]. Other famous examples are synthetic life-inspired transcriptional oscillators [5–7]. In chemistry, extensive experimental and theoretical work has revealed the underlying mechanism of oscillating chemical reactions, with such as the Briggs–Rauscher reaction [8,9], the Belousov-Zhabotinsky reaction [10,11], and the Brusselator [12,13] as paradigm examples. The oscillations emerge as a consequence of nonlinearities in the chemical rates, giving rise to an unstable region in phase space, typically through a Hopf-bifurcation [14,15]. Such nonlinearities can further lead to excitable concentration fronts and pulses, and stationary Turing patterns [16–20].

An alternative mechanism for spatial patterns in chemically active systems is through phase separation of liquid condensates [21–24]. The patterns in phase-separated systems do not require nonlinearities in the chemical rates—attractive interactions between the components give rise to a phase boundary mediating nonlinear transport [25–27]. When the chemical reactions break detailed balance of the rates, the system is maintained away from equilibrium, making the droplets active [25,28,29]. Active droplets can behave fundamentally different from their equilibrium counterpart, exhibiting properties such as droplet division [30], accelerated ripening [31], size control [30,32,33], shell-formation [34], and various other spatial morphologies [35–37].

An open question is whether liquid droplets can undergo oscillation with cycles of droplet formation and dissolution [38–40]. Our Letter presents a minimal and experimentally inspired theoretical model to achieve self-sustained oscillation of condensates cycling between their formation and dissolution; see Fig. 1. We show that a saddle-node bifurcation emerges as active droplets are driven far away from equilibrium. With the addition of a second reaction, the droplets behave as an excitable medium, exhibiting both wave propagation and self-sustained oscillations.

Theory of active droplets—The evolution of volume fractions $\phi_i(\boldsymbol{x}, t)$ in space $\boldsymbol{x}$ and time t are governed by diffusive fluxes $\boldsymbol{j}_i$ and reaction rates r_i of component i with the corresponding continuous equations [25,40,41]

$$\partial_t \phi_i(\boldsymbol{x}, t) = -\nabla \cdot \boldsymbol{j}_i + r_i, \qquad i = A, B. \tag{1}$$

We consider a ternary mixture (A, B, C) with $\phi_C = 1 - \phi_A - \phi_B$. Initially, we account for a reversible unimolecular chemical reaction between A and B,

$$r_1 : A \underset{k_1}{\overset{k_1 \exp\{\tilde{\delta}/(k_B T)\}}{\rightleftharpoons}} B, \tag{2}$$

where the net reaction rate $r_1 := r_B = -r_A$, and k_1 is the reaction rate coefficient. The reaction rates are governed by the chemical potentials $\mu_i = (\partial G/\partial N_i)_{N_{j\neq i}, p, T}$, where G is the Gibbs free energy [42,43], such that

*Contact author: christoph.weber@uni-a.de

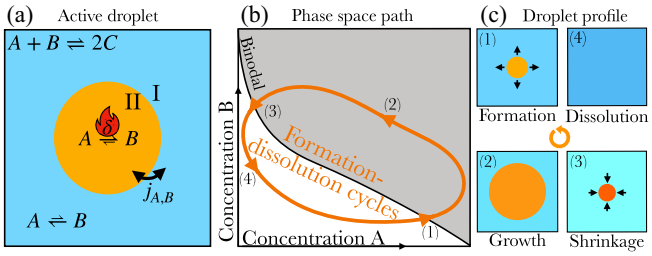

FIG. 1. Formation and dissolution of active droplets: (a) Chemically active droplets break detailed balance of the rates by the turnover of a fuel δ [Eq. (2)]. This fuel drives the turnover of component A to B in the dense phase (II), while in the dilute phase (I), there is no fuel, and the pathway from B to A dominates. We find that for a large enough fuel strength δ, a saddle-node bifurcation occurs, making the system bistable. (b) Through an additional reaction [Eq. (12)], the active droplet can become excitable and capable of self-sustained cycles (c): they form (1) and grow (2), before shrinking (3) and dissolving (4), starting the cycle again.

$$r_1 = k_1\left[\exp\left\{\frac{\mu_A + \tilde{\delta}(\phi_A,\phi_B)}{k_BT}\right\} - \exp\left\{\frac{\mu_B}{k_BT}\right\}\right], \quad (3)$$

where k_BT is the thermal energy. Moreover, $\tilde{\delta}(\phi_A,\phi_B)$ captures the effects of a fuel [44,45] that enhances the forward reaction pathway, where $\exp\{\tilde{\delta}/(k_BT)\}$ can be understood as a chemostatted fuel activity; see Supplemental Material (SM) [46] for details. The fuel breaks detailed balance of the rates [25,49], $r_1^{\rightharpoonup}/r_1^{\leftharpoondown} = \exp\{(\Delta\mu + \tilde{\delta})/(k_BT)\}$, where $\Delta\mu = \mu_A - \mu_B$ is the thermodynamic force of the reaction, which vanishes at equilibrium ($\Delta\mu = 0$).

According to Eq. (1), the volume fraction fields ϕ_i further evolve due to chemical potential gradients in space, creating diffusive fluxes $\boldsymbol{j}_i = -\sum_j \Lambda_{ij}\nabla\mu_j$, where Λ_{ij} are the mobility coefficients [50]. Sufficiently strong interactions between the components leads to phase separation, creating stable inhomogeneous volume-fraction profiles.

The dynamic equation (1) can be reduced [43] when the diffusive timescales over the system of size L are much faster than the reaction timescale $k_1 \ll \Lambda_i/(k_BTL^2)$. In this limit, each phase is homogeneous in composition with different volume fractions in each phase $(\phi_i^{\mathrm{I}}, \phi_i^{\mathrm{II}})$ with corresponding phase volumes V^{I} and $V^{\mathrm{II}} = V - V^{\mathrm{I}}$, where V is the system volume. Strikingly, the chemical kinetics can be represented as a trajectory of average volume fractions in the thermodynamic phase diagram; see, e.g., Fig. 1 for a cycling trajectory (orbit) in a phase diagram where A and B can phase separate from the solvent C. The phase composition (I,II) "live" on the binodal line and satisfy phase equilibrium, $\mu_i^{\mathrm{I}} = \mu_i^{\mathrm{II}}$, at all times. The reduced dynamic equations in each phase are [43]

$$\frac{\mathrm{d}\phi_i^{\mathrm{I/II}}}{\mathrm{d}t} = r_i^{\mathrm{I/II}} - j_i^{\mathrm{I/II}} - \phi_i^{\mathrm{I/II}}\frac{\dot{V}^{\mathrm{I/II}}}{V^{\mathrm{I/II}}}, \quad (4a)$$

$$\frac{\dot{V}^{\mathrm{I/II}}}{V^{\mathrm{I/II}}} = \sum_{k=A,B,C}\left(r_k^{\mathrm{I/II}} - j_k^{\mathrm{I/II}}\right), \quad (4b)$$

where $i = A$, B, and the diffusive flux $j_i^{\mathrm{I/II}}$ ensures the conditions of phase coexistence; see SM [46] for a derivation. Phase-averaged quantities are denoted by a bar, which, for an arbitrary quantity X at phase equilibrium, is

$$\bar{X} \equiv \frac{V^{\mathrm{I}}X^{\mathrm{I}} + V^{\mathrm{II}}X^{\mathrm{II}}}{V^{\mathrm{I}} + V^{\mathrm{II}}}. \quad (5)$$

For a ternary system with chemical reaction 1 [Eq. (2)], a natural choice of quantities is the phase-averaged total volume fraction $\bar{\psi}$, which is conserved during reaction 1, and the phase-averaged reaction extent $\bar{\xi}$,

$$\bar{\psi} \equiv \frac{\bar{\phi}_A + \bar{\phi}_B}{2}, \qquad \bar{\xi} \equiv \frac{\bar{\phi}_B - \bar{\phi}_A}{2}. \quad (6)$$

With this choice of quantities, Eq. (4) become

$$\mathrm{d}_t\bar{\psi} = 0, \qquad \mathrm{d}_t\bar{\xi} = \bar{r}_1. \quad (7)$$

Steady states, which corresponds to $\bar{r}_1 = 0$, defines the reaction nullcline of r_1:

$$V^{\mathrm{I}}r_1^{\mathrm{I}} + V^{\mathrm{II}}r_1^{\mathrm{II}} = 0. \quad (8)$$

For chemical reactions with phase-dependent fueling, such that $\tilde{\delta}^{\mathrm{I}} \neq \tilde{\delta}^{\mathrm{II}}$, the nullcline for phase-separated systems depends on the phase volumes, which is not the case without fuel ($\tilde{\delta} = 0$). The system is kept away from equilibrium by the composition-dependent fueling

$$\tilde{\delta}(\psi) = \frac{\delta}{2}\left[1 + \tanh\left(\frac{\psi - \psi_\delta}{\kappa}\right)\right], \quad (9)$$

where $\delta \geq 0$ is the fuel strength that enhances turnover from A to B. For $\delta = 0$, the system can settle to thermodynamic equilibrium. The parameter $\kappa \ll 1$ sets the range of ψ values where the system transitions from unfueled to fueled, centered around ψ_δ. We choose $\psi_\delta = 0.25$ such that the dilute phase is approximately unfueled, while the dense phase is fueled ($\tilde{\delta}^{\mathrm{I}} \simeq 0, \tilde{\delta}^{\mathrm{II}} \simeq \delta$). The phase-dependent fueling gives rise to nonequilibrium steady states (NESS) with continuous chemical turnover in both phases, which is balanced by diffusive exchange between the phases. From Eq. (8), we find that the balance occurs for droplet volumes satisfying

$$\frac{V^{\mathrm{II}}}{V} = \frac{k_1^{\mathrm{I}}\left[e^{\frac{\Delta\mu+\delta^{\mathrm{I}}}{k_BT}} - 1\right]}{k_1^{\mathrm{I}}\left[e^{\frac{\Delta\mu+\delta^{\mathrm{I}}}{k_BT}} - 1\right] - k_1^{\mathrm{II}}\left[e^{\frac{\Delta\mu+\delta^{\mathrm{II}}}{k_BT}} - 1\right]}, \quad (10)$$

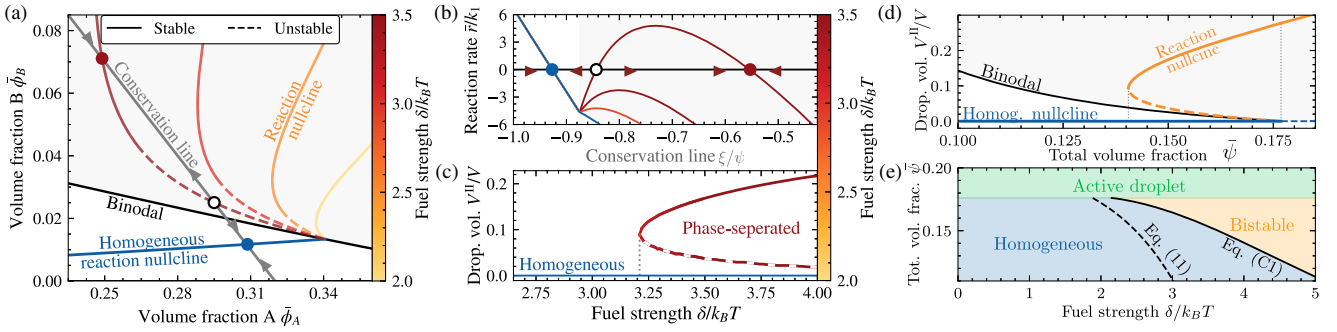

FIG. 2. Subcritical saddle-node bifurcation to an active droplet: (a) Upon increasing the fuel strength δ, the reaction nullcline [Eq. (10)] for reaction r_1 [Eq. (2)] in the phase-separated domain (gray shaded, binodal black line) bends, leading to three nonequilibrium steady states (NESS) for a fixed conservation line $\bar{\psi} = 0.16$; closed symbols are stable and open symbols unstable fixed points. (b) The phase averaged reaction rate [Eq. (5)] along the same conservation line only has multiple steady states for sufficiently large fuel strength $\delta/(k_BT)$, where the center point is unstable. (c) The multiple steady points arise from a subcritical saddle-node bifurcation with a jump in droplet volume above a critical fuel strength δ^* (vertical dotted line). Above this threshold value δ^*, there are three NESS where two are locally stable (bistability). (d) At a fixed fuel strength ($\delta = 4k_BT$), the bifurcation depends on the value of quantity $\bar{\psi}$ conserved by reaction [Eq. (2)]. There is a range of $\bar{\psi}$-values (vertical dotted lines), where the system is bistable, which grows with fuel strength δ. (e) The bistable region in $\bar{\psi}$ grows with fuel strength δ, and the transition to bistability at δ^* [solid black line, Eq. (C1)] is accurately captured by the approximate expression [solid dashed line, Eq. (11)] near the minimal fuel strength but deviates at lower $\bar{\psi}$.

where $\delta^{\mathrm{I/II}} = \tilde{\delta}(\psi^{\mathrm{I/II}})$ and $k_1^{\mathrm{I/II}}$ denote the phase-dependent reaction rate coefficients of reaction 1 [Eq. (2)]. Without fuel, all volumes for the tie line of $\Delta\mu = 0$ is at equilibrium. Unless stated otherwise, we solve Eq. (4) numerically [48]; see SM [46] for parameters used.

Saddle-node bifurcation to an active droplet—We consider a phase diagram and a conserved quantity $\bar{\psi}$ for which the steady state is homogeneous, thermodynamic equilibrium state in the absence of fuel ($\delta = 0$). Upon increasing the fuel strength δ, active droplets emerge as locally stable steady states. Their emergence requires sufficient fueling to bend the reaction nullcline strongly [Figs. 2(a) and 2(b)], creating multiple intersections with the conserved line of constant total volume fraction $\bar{\psi}$. Since the homogeneous steady state remains stable as δ increases, the additional stable active droplet state makes the system bistable.

The bistability between an active droplet state and a homogeneous state for increasing δ emerges through a subcritical saddle-node bifurcation at which the steady droplet volume V^{II} jumps from zero to a finite value; see Fig. 2(c) and the normal form derived in Appendix A. The bifurcation occurs at a critical fuel strength δ^*, approximately given by

$$\delta^* \simeq k_BT \log\left(1 + \Theta + \frac{\psi^{\mathrm{I}} - \bar{\psi}}{\psi^{\mathrm{II}} - \psi^{\mathrm{I}}}\Theta^2\right), \tag{11}$$

where Θ is a function depending solely on thermodynamic parameters [see Appendix C, Eq. (C4)] and the equation holds for $\bar{\psi} < \psi^{\mathrm{I}}$. The bifurcation requires $\Theta > 0$ corresponding to specific phase diagram types and, equivalently, specific interactions in mixture. The case $\Theta > 0$ is realized when the product (B) of the fueled reaction phase separates more strongly from the solvent than its precursor (A), implying $\chi_{BC} > \chi_{AC}$, as is the case in Figs. 1 and 2. Since Θ cannot approach zero, the fuel is a prerequisite for the bistability.

Bistability is only possible in a range of total volume fractions $\bar{\psi}$ values, and this range increases with fuel strength δ [orange domain in Figs. 2(d) and 2(e)]. The minimal fuel necessary to trigger the bistability is well captured by δ^* [Eq. (11)] near the minimal fuel strength; see Fig. 2(e). When the fuel strength is fixed, we find that bistability requires large enough values of the total volume fraction $\bar{\psi}$ [Fig. 2(d)]. There is a jump of both phase volume and average composition, indicating a saddle-node bifurcation when varying $\bar{\psi}$.

Excitable active droplet—Excitable systems can lead to wave propagation upon a perturbation, followed by a refractory period in which the system is no longer excitable [16–18,51]. Here, we show that the bistable system discussed in the previous paragraph becomes excitable upon adding a second reaction r_2 changing the otherwise conserved quantity $\bar{\psi}$ [Eq. (6)] in time,

$$r_2\colon\ A + B \underset{k_2}{\rightleftharpoons} 2C. \tag{12}$$

The stoichiometric factor of 2 results from our choice of equal molecular volumes, ensuring that the reaction is volume conserving. Note that C represents an effective component of both solvent and a weakly interacting chemically reacting component, allowing us to maintain a minimalistic description. Reaction 2,

$$r_2 = k_2\left(\exp\left\{\frac{2\mu_C}{k_BT}\right\} - \exp\left\{\frac{\mu_A + \mu_B}{k_BT}\right\}\right), \tag{13}$$

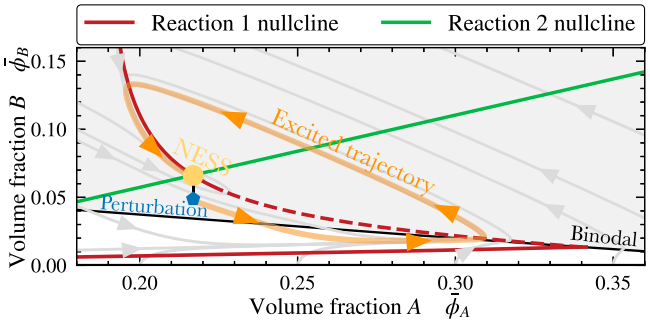

FIG. 3. Excitable active droplet. When considering the reactions r_1 [Eq. (2)] and reaction r_2 [Eq. (13)], the active droplet system becomes excitable. A compositional perturbation (blue pentagon) can excite the system. As a result, the system follows an extended trajectory (orange) far beyond the initial perturbation. During this excited trajectory, the system has a refractory period when it is no longer excitable. It relaxes back to the NESS (yellow circle), where the reaction nullclines for both reactions intersect (green and red lines). The active droplet system is a bistable excitable media.

obeys detailed balance of the rates and makes the net reaction rates r_i in Eqs. (1) and (4) $r_A = r_2 - r_1$ and $r_B = r_2 + r_1$. The dynamics of the average reaction extent and the total volume fraction [Eq. (6)] become

$$\mathrm{d}_t\bar{\xi} = \bar{r}_1, \qquad \mathrm{d}_t\bar{\psi} = \bar{r}_2. \tag{14}$$

For a bistable droplet [$\delta > \delta^*$, Eq. (11)], we find that certain compositional perturbations reducing the droplet volume can destabilize it, leading to an excited trajectory (Fig. 3). Such a perturbation initially leads to the dissolution of the droplet. Once dissolved, the reactions drive the average composition into the binodal, nucleating an active droplet, and returning the system to its initial nonequilibrium steady state. Along its excited trajectory, the system exhibits a refractory period when it is no longer excitable. The resulting evolution of the droplet volume in time is reminiscent of a wave pulse.

Oscillating active droplet—When the excitable fixed point becomes unstable, the active droplet undergoes cycles of formation and dissolution. Graphically, destabilization occurs when the nullclines of r_2 intersect the unstable part of the nullcline of r_1. When this occurs, the droplet grows after nucleation as fueling favors the conversion of A to B [Fig. 4(b)]. As the composition shifts, the net reaction rate $\bar{r}_2$ changes sign, reducing the total volume fraction $\bar{\psi}$ and shrinking the droplet until it crosses the unstable branch of the saddle-node bifurcation [Figs. 2(c) and 2(d), dashed lines]. The droplet then dissolves, fueling ceases, and $\bar{r}_1$ reverses, converting B back to A. Now r_2 has changed sign, leading to droplet nucleation, restoring the initial state, and the cycle repeats. In other words, the oscillations emerge because the attractor lies within the binodal while the system is homogeneous, but once a droplet nucleates, the phase-dependent fuel shifts the attractor outside the binodal.

The transition between an excitable system (Fig. 3) to a system with an oscillating active droplet [Fig. 4(a)] corresponds to a Hopf bifurcation [14–16,51]. At the Hopf bifurcation, eigenvalues of the linearization around the fixed point become imaginary, which can for example be triggered by increasing the fuel strength δ.

The Hopf bifurcation can be understood through the system's normal form [Eq. (14)]. It is obtained by performing a Taylor expansion on both sides of the binodal (see SM [46] for the derivation), yielding

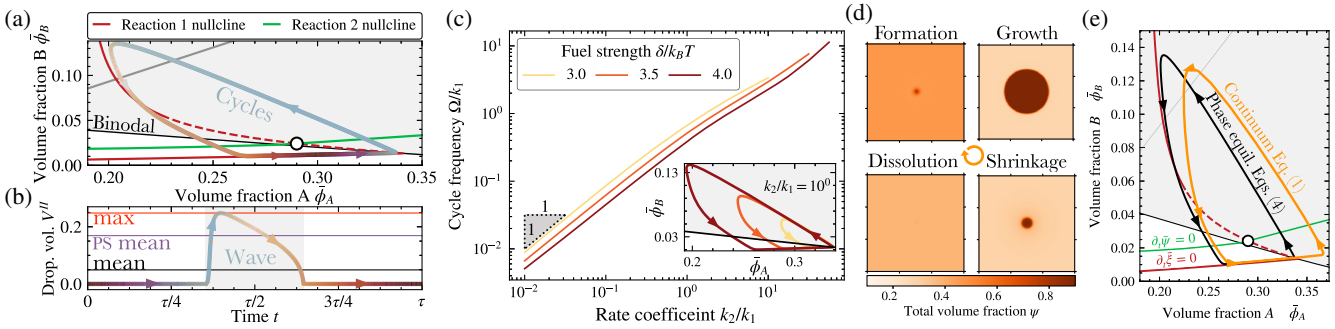

FIG. 4. Self-sustained cycles of droplet formation and dissolution: (a) for cases where the intersection between the two reaction nullclines (green and red lines) occurs for unstable droplet volumes (white dot), it cannot concomitantly satisfy its two steady-state conditions. The result is self-sustained oscillations of an active droplet cycling between formation and dissolution. (b) When nucleated at the same position, droplet formation and dissolution correspond to a standing wave. (c) The cycle frequency Ω is weakly affected by the fuel strength δ. However, the cyclic trajectories in phase space (inset) are significantly bigger. The cycle frequency follows a power-law with the reaction rate coefficient k_2, $\Omega \propto k_2$, due to the fuel making r_1 relax much faster than r_2 upon formation and dissolution. (d),(e) We confirm active droplets' formation and dissolution cycles by solving the continuum equation for the volume fraction fields [Eq. (1)] numerically. We find a good agreement of the phase space trajectory of the spatially averaged volume fractions for phase equilibrium theory [Eq. (4)]. An animation corresponding to panel (d) is included in SM [46].

$$\mathrm{d}_t\bar{\psi} \simeq -(\bar{\xi}-\bar{\xi}_1)f_\xi - (\bar{\psi}-\bar{\psi}_1)f_\psi,$$
$$\mathrm{d}_t\bar{\xi} \simeq \begin{cases} -(\bar{\psi}-\bar{\psi}_0)h_\psi - (\bar{\xi}-\bar{\xi}_0)h_\xi, & \bar{\xi} \le \xi^{\mathrm{I}}, \\ \bar{r}_1 - (\bar{\psi}-\bar{\psi}_1)\tilde{h}_\psi - h_{\xi\xi}(\bar{\xi}-\bar{\xi}_2)^2, & \bar{\xi} > \xi^{\mathrm{I}}. \end{cases} \quad (15)$$

We find that $f_\xi > 0$, $h_\psi < 0$, and $\tilde{h}_\psi > 0$, leads to negative feedback between $\bar{\psi}(t)$ and $\bar{\xi}(t)$ (for definitions and discussions see SM [46]). The signs of f_ξ and h_ψ are set by thermodynamics, while the difference in sign between $\tilde{h}_\psi$ and h_ψ occurs due to fueling. Negative feedback, together with the instability at the intersection of the two nullclines, is the fundamental ingredient for the emergence of oscillations in nonlinear systems [16,52].

The oscillation frequency is dominantly set by the reaction rate coefficient k_2 of the second reaction (13). This property is apparent in the scaling of the cycle frequency $\Omega \propto k_2$, as shown in Fig. 4(c). The dominant role of k_2 arises because the fueled reaction is fast upon droplet nucleation and dissolution. The slower unfueled reaction 2, with $k_2 \ll k_1 \exp\delta/(k_BT)$, thus becomes rate-limiting and sets the cycle frequency Ω. Accordingly, variations in the fuel strength δ only weakly affect the cycle frequency Ω, while the compositional changes along a cycle become more pronounced for larger δ [Fig. 4(c), inset and Appendix B].

Consistently, we find formation-dissolution cycles when numerically [53] solving the continuous dynamic equations (numerical details see Refs. [46,48]) for the volume fraction fields $\phi_i(\boldsymbol{x}, t)$ [Eq. (1)]. Figure 4(d) depicts representative snapshots of the volume fraction fields indicating the formation, growth, shrinkage, and dissolution of an active droplet over the period $(2\pi/\Omega)$, where a localized external potential is included to mimic a nucleation site (see SM [46] for details). Figure 4(e) shows the corresponding phase diagram trajectory, which agrees well with the fast-diffusion limit. We conclude that the self-sustained oscillations are well captured by the dynamics in the fast-diffusion limit [Eq. (4)] that paved the way to determine the normal forms of the underlying Hopf bifurcation [Eq. (15)].

Discussion—We show that droplet oscillations can occur through a combination of minimalistic chemistry and phase separation, which can be realized experimentally by satisfying the following requirements: (i) a fuel-driven reaction cycle must regulate the product composition by converting molecule A into B using a chemical fuel. Such schemes have been demonstrated using carbodiimides [54,55] or phosphorylating agents [56–58] to activate droplet-forming molecules like peptides or oils [59]. For example, a positively charged peptide (A) forms coacervate droplets with RNA [60]; upon carbodiimide activation, it becomes more charged, and B partitions more strongly into the droplets. (ii) Activation should occur mainly inside the droplets, which can be ensured if the fuel partitions preferentially into them. For example, using coacervates with positively charged molecules enables typically negatively charged fuels to accumulate within, driving activation inside. (iii) The activated molecule B must spontaneously deactivate back to A, preferably outside the droplets. In carbodiimide systems, this occurs via hydrolysis; localization can be tuned using catalysts or enzymes that remain in the dilute phase. (iv) Finally, A and B should react reversibly to form C, which does not partition into droplets. This can occur through transacylation, where anhydride B reacts with A to form a mixed anhydride C [61], predominantly inside droplets.

Oscillating droplet systems could be used to design lifelike systems such as synthetic cells and *de novo* active matter [39,62]. Oscillations can prevent behaviors on long timescales in phase-separated systems, such as ripening in living cells through noisy oscillators [63]. Theoretical studies showed that oscillating DNA-repair condensates enhance the efficiency of the DNA damage response, and experiments revealed that oscillatory dynamics of p53 directly promote DNA repair [64]. Consistent with this view, recent observations hint that p53 oscillations also manifest as oscillatory condensates [65].

Acknowledgments—We thank Leonardo Silva Dias for careful feedback on the manuscript and his recommendations for references on chemical oscillators. C. A. W. acknowledges the European Research Council (ERC) under the European Union's Horizon 2020 research and innovation program (Fuelled Life, Grant No. 949021), and the SPP 2191 "Molecular Mechanisms of Functional Phase Separation" of the German Science Foundation for financial support.

Data availability—The data that support the findings of this article are openly available [47], embargo periods may apply.

[1] W. A. Zehring, D. A. Wheeler, P. Reddy, R. J. Konopka, C. P. Kyriacou, M. Rosbash, and J. C. Hall, Cell **39**, 369 (1984).
[2] T. A. Bargiello, F. R. Jackson, and M. W. Young, Nature (London) **312**, 752.
[3] J. C. Dunlap, Cell **96**, 271 (1999).
[4] A. Goldbeter, *Biochemical Oscillations and Cellular Rhythms: The Molecular Bases of Periodic and Chaotic Behaviour* (Cambridge University Press, Cambridge, England, 1996).
[5] M. B. Elowitz and S. Leibler, Nature (London) **403**, 335 (2000).
[6] J. Stricker, S. Cookson, M. R. Bennett, W. H. Mather, L. S. Tsimring, and J. Hasty, Nature (London) **456**, 516 (2008).
[7] J. Kim and E. Winfree, Mol. Syst. Biol. **7**, 465 (2011).
[8] W. C. Bray, J. Am. Chem. Soc. **43**, 1262 (1921).
[9] A. M. Zhabotinsky, Chaos **1**, 379 (1991).
[10] A. Pechenkin, J. Biosci. **34**, 365 (2009).
[11] B. P. Belousov, A periodic reaction and its mechanism, in *Sbornik Referatov po Radiatsionnoi Meditsine* (Medgiz, Moscow, 1959); A. M. Zhabotinsky, Biofizika **9**, 306 (1964).
[12] I. Prigogine and G. Nicolis, J. Chem. Phys. **46**, 3542 (1967).
[13] I. Prigogine and R. Lefever, J. Chem. Phys. **48**, 1695 (1968).

[14] J. E. Marsden and M. McCracken, *The Hopf Bifurcation and its Applications* (Springer Science & Business Media, New York, 2012).
[15] T. Caraballo, J. A. Langa, and J. C. Robinson, Proc. R. Soc. A **457**, 2041 (2001).
[16] M. C. Cross and P. C. Hohenberg, Rev. Mod. Phys. **65**, 851 (1993).
[17] A. M. Turing, Phil. Trans. R. Soc. B **237**, 37 (1997).
[18] I. R. Epstein and K. Showalter, J. Phys. Chem. **100**, 13132 (1996).
[19] B. Novák and J. J. Tyson, Nat. Rev. Mol. Cell Biol. **9**, 981 (2008).
[20] J. Halatek and E. Frey, Nat. Phys. **14**, 507 (2018).
[21] J. Söding, D. Zwicker, S. Sohrabi-Jahromi, M. Boehning, and J. Kirschbaum, Trends Cell Biol. **30**, 4 (2020).
[22] A. W. Folkmann, A. Putnam, C. F. Lee, and G. Seydoux, Science **373**, 1218 (2021).
[23] A. A. Hyman, C. A. Weber, and F. Jülicher, Annu. Rev. Cell Dev. Biol. **30**, 39 (2014).
[24] S. F. Banani, H. O. Lee, A. A. Hyman, and M. K. Rosen, Nat. Rev. Mol. Cell Biol. **18**, 285 (2017).
[25] C. A. Weber, D. Zwicker, F. Jülicher, and C. F. Lee, Rep. Prog. Phys. **82**, 064601 (2019).
[26] C. Luo and D. Zwicker, Phys. Rev. E **108**, 034206 (2023).
[27] L. Menou, C. Luo, and D. Zwicker, J. R. Soc. Interface **20**, 20230244 (2023).
[28] B. Rieß, R. K. Grötsch, and J. Boekhoven, Chem **6**, 552 (2020).
[29] D. Zwicker, arXiv:2407.09859.
[30] D. Zwicker, R. Seyboldt, C. A. Weber, A. A. Hyman, and F. Jülicher, Nat. Phys. **13**, 408 (2017).
[31] M. Tena-Solsona, J. Janssen, C. Wanzke, F. Schnitter, H. Park, B. Rieß, J. M. Gibbs, C. A. Weber, and J. Boekhoven, ChemSystemsChem **3**, e2000034 (2021).
[32] J. D. Wurtz and C. F. Lee, Phys. Rev. Lett. **120**, 078102 (2018).
[33] D. Zwicker, A. A. Hyman, and F. Jülicher, Phys. Rev. E **92**, 012317 (2015).
[34] A. M. Bergmann, J. Bauermann, G. Bartolucci, C. Donau, M. Stasi, A.-L. Holtmannspötter, F. Jülicher, C. A. Weber, and J. Boekhoven, Nat. Commun. **14**, 6552 (2023).
[35] G. Bartolucci, O. Adame-Arana, X. Zhao, and C. A. Weber, Biophys. J. **120**, 4682 (2021).
[36] I. B. A. Smokers, B. S. Visser, W. P. Lipiński, K. K. Nakashima, and E. Spruijt, ChemSystemsChem **7**, e202400056 (2025).
[37] J. Bauermann, G. Bartolucci, J. Boekhoven, F. Jülicher, and C. A. Weber, Phys. Rev. X **15**, 041027 (2025).
[38] T. Mittag and R. V. Pappu, Mol. Cell **82**, 2201 (2022).
[39] E. Spruijt, Commun. Chem. **6**, 23 (2023).
[40] F. Jülicher and C. A. Weber, Annu. Rev. Condens. Matter Phys. **15**, 237 (2024).
[41] J. Bauermann, C. A. Weber, and F. Jülicher, Ann. Phys. (Amsterdam) **534**, 2200132 (2022).
[42] O. Adame-Arana, C. A. Weber, V. Zaburdaev, J. Prost, and F. Jülicher, Biophys. J. **119**, 1590 (2020).
[43] J. Bauermann, S. Laha, P. M. McCall, F. Jülicher, and C. A. Weber, J. Am. Chem. Soc. **144**, 19294 (2022).
[44] J. Boekhoven, A. M. Brizard, K. N. K. Kowlgi, G. J. M. Koper, R. Eelkema, and J. H. van Esch, Angew. Chem. **122**, 4935 (2010).
[45] J. Boekhoven, W. E. Hendriksen, G. J. M. Koper, R. Eelkema, and J. H. van Esch, Science **349**, 1075 (2015).
[46] See Supplemental Material at http://link.aps.org/supplemental/10.1103/g9dh-ymx9 for additional information, animations, definitions, and derivations. The corresponding dataset can be fond in Ref. [47], with all code available in Ref. [48].
[47] C. A. Weber and I. S. Haugerud, Excitability and oscillations of active droplets, 10.5281/zenodo.19612876 (2026).
[48] I. Haugerud, Excitability and oscillations of active droplets, https://github.com/ivarhaugerud/Excitability-and-oscillations-of-active-droplets (2025), accessed: April 2026, 17.
[49] F. Jülicher, A. Ajdari, and J. Prost, Rev. Mod. Phys. **69**, 1269 (1997).
[50] S. R. De Groot and P. Mazur, *Non-Equilibrium Thermodynamics* (Courier Corporation, Amsterdam, 2013).
[51] M. Cross and H. Greenside, *Pattern Formation and Dynamics in Nonequilibrium Systems* (Cambridge University Press, Cambridge, England, 2009).
[52] S. H. Strogatz, *Nonlinear Dynamics and Chaos with Student Solutions Manual: With Applications to Physics, Biology, Chemistry, and Engineering* (CRC Press, Boca Raton, FL, 2018).
[53] J. Zhu, L.-Q. Chen, J. Shen, and V. Tikare, Phys. Rev. E **60**, 3564 (1999).
[54] C. Donau, F. Späth, M. Sosson, B. A. Kriebisch, F. Schnitter, M. Tena-Solsona, H.-S. Kang, E. Salibi, M. Sattler, H. Mutschler *et al.*, Nat. Commun. **11**, 5167 (2020).
[55] F. Späth, C. Donau, A. M. Bergmann, M. Kraänzlein, C. V. Synatschke, B. Rieger, and J. Boekhoven, J. Am. Chem. Soc. **143**, 4782 (2021).
[56] K. K. Nakashima, M. H. van Haren, A. A. André, I. Robu, and E. Spruijt, Nat. Commun. **12**, 3819 (2021).
[57] S. M. Poprawa, M. Stasi, B. A. Kriebisch, M. Wenisch, J. Sastre, and J. Boekhoven, Nat. Commun. **15**, 4204 (2024).
[58] W. M. Aumiller, Jr. and C. D. Keating, Nat. Chem. **8**, 129 (2016).
[59] C. Donau and J. Boekhoven, Trends Chem. **5**, 45 (2023).
[60] F. Späth, A. S. Maier, M. Stasi, A. M. Bergmann, K. Halama, M. Wenisch, B. Rieger, and J. Boekhoven, Angew. Chem., Int. Ed. Engl. **62**, e202309318 (2023).
[61] F. Späth, H. Soria-Carrera, M. Stasi, J. Sastre, B. A. Kriebisch, and J. Boekhoven, Angew. Chem., Int. Ed. Engl. **63**, e202407424 (2024).
[62] C. M. E. Kriebisch *et al.*, Chem **11**, 102399 (2025).
[63] V. T. Yan, A. Narayanan, T. Wiegand, F. Jülicher, and S. W. Grill, Nature (London) **609**, 597 (2022).
[64] M. S. Heltberg, A. Lucchetti, F.-S. Hsieh, D. P. M. Nguyen, S.-h. Chen, and M. H. Jensen, Cell **185**, 4394 (2022).
[65] M. S. Heltberg, Y. Jiang, Y. Fan, Z. Zhang, M. S. Nordentoft, W. Lin, L. Qian, Q. Ouyang, M. H. Jensen, and P. Wei, Cell Syst. **14**, 382 (2023).
[66] F. Jülicher and J. Prost, Eur. Phys. J. E **29**, 27 (2009).

End Matter

Appendix A: Bistable normal form—The onset of bistability can be understood through a normal form obtained from Taylor expanding the dynamic Eq. (7) for the reaction extent $\bar{\xi}$. By expanding the phase-separated and homogeneous case separately, at the points $(\bar{\xi}_0, \bar{\psi}_0)$ and $(\bar{\xi}_2, \bar{\psi}_0)$ respectively, we find

$$\mathrm{d}_t\bar{\xi} \simeq \begin{cases} -(\bar{\xi}-\bar{\xi}_0)h_1, & \bar{\xi} \le \xi^{\mathrm{I}}, \\ \bar{r}_1(\bar{\xi}_2, \bar{\psi}_0) - (\bar{\xi}-\bar{\xi}_2)^2 h_2 & \bar{\xi} > \xi^{\mathrm{I}}, \end{cases} \tag{A1}$$

with the coefficients h_1 and h_2 derived in [46], $\bar{r}_1$ is the phase-averaged reaction rate evaluated at the phase-separated expansion point, and ξ^{I} is the reaction extent at the dilute branch of the binodal for the given $\bar{\psi}_0$. As seen in Fig. 2(b), for homogeneous values of the reaction extent ($\bar{\xi} \le \xi^{\mathrm{I}}$), the reaction rate is linear and stable ($h_1 > 0$) around its steady point $\bar{\xi}_0$. For phase-separated values of the reaction extent ($\bar{\xi} > \xi^{\mathrm{I}}$), a second-order expansion is necessary to capture the behaviour for strong fueling $\delta \gg k_{\mathrm{B}}T$. Since the normal form in the phase-separated domain corresponds to a concave parabola ($h_2 > 0$), the requirement for bistability is a positive offset value at the expansion point:

$$\bar{r}_1 = \overrightarrow{r_1}\left(\overline{\exp\left\{\frac{\delta}{k_BT}\right\}} - \exp\left\{-\frac{\Delta\mu}{k_BT}\right\}\right) > 0. \tag{A2}$$

This equation shows that the saddle-node bifurcation occurs when the thermodynamic force $\Delta\mu$ is dominated by the nonequilibrium driving δ. The bar denotes a phase average [Eq. (5)]. We note that for $\bar{\psi}_0$ values with a homogeneous steady point, the chemical potential difference is negative when phase separated ($\Delta\mu < 0$).

Appendix B: Entropy production—The entropy production characterizes the system's dissipation and serves as a measure of how far a system is away from thermodynamic equilibrium [49]. For the case of the active droplet, entropy is produced due to the detailed-balance broken chemical reaction [Eq. (3) with $\tilde{\delta} \neq 0$]. Specifically, the entropy production originates from the fact that the fuel is chemostatted, implying an entropy-producing boundary flux to maintain a chemostatted fuel. The entropy production rate $\dot{s}$ follows [41,66]

$$-T\partial_t s = \partial_t g + j_F, \tag{B1}$$

where s is the entropy density and g is the Gibbs free energy density, see SM [46] for definitions. The flux of fuel into the system j_F balances the loss of fuel by the fueled reaction, $j_F = -\mu_F r_F/\nu_F$, where we now explicitly keep track of the chemostatted fuel with a constant chemical potential μ_F and molecular volume ν_F. In a nonequilibrium steady state $\partial_t g = 0$, and it further integrates to zero over a closed cycle, such that all entropy production originates from the dissipative fueled reaction j_F. From the fueled reaction rate r_F (see SM [46] for derivation), we find

$$\frac{\dot{s}}{k_B} = \frac{\mu_F k_{\mathrm{f}}}{k_BT\nu_F}\exp\left\{\frac{\mu_A+\mu_F}{k_BT}\right\}. \tag{B2}$$

Performing a volume integral to find the entropy production rate $\dot{S} = \int \dot{s}\mathrm{d}^3x$ yields

$$\frac{\dot{S}}{k_B} = \frac{\mu_F}{k_BT\nu_F}\exp\left\{\frac{\mu_A+\mu_F}{k_BT}\right\}(V^{\mathrm{I}}k_{\mathrm{f}}^{\mathrm{I}} + V^{\mathrm{II}}k_{\mathrm{f}}^{\mathrm{II}}). \tag{B3}$$

At a nonequilibrium steady state, we can use the expression of the droplet volume V^{II} [Eq. (10)] and the relation between fuel strength $\tilde{\delta}$ and k_{f} (see SM [46]), where $\tilde{\delta}^{\mathrm{I}} = 0$ and $\tilde{\delta}^{\mathrm{II}} = \delta$. The entropy production at the nonequilibrium steady state simplifies to

$$\frac{\dot{S}_{\mathrm{NESS}}}{k_B} = \frac{\mu_F k_1 V}{k_BT\nu_F}\left(\exp\left\{\frac{\mu_B}{k_BT}\right\} - \exp\left\{\frac{\mu_A}{k_BT}\right\}\right). \tag{B4}$$

Interestingly, the entropy production is independent of the fuel strength δ and the phase volumes. This result is depicted in Fig. 5, where the entropy production density in the NESS does not increase with the fuel strength δ when phase separated. The dissipation being fuel-strength independent for active droplets occurs due to the chemical reaction r_2 [Eq. (12)] obeying detailed balance of the rates, such that the chemical potentials μ_A and μ_B are fixed by the tie-line selected through the nullcline of r_2 [green line in Figs. 3 and 4(a)]. Thus, the entropy production for active droplets is independent of the fuel strength δ, and is instead a constant set by the properties of the nondissipative chemical reaction 2. For a fixed $\Delta\mu = \mu_A - \mu_B$, we see from Eq. (10) that an increase in fuel strength δ^{II} decreases the droplet volume. This reduced volume exactly balances the increased dissipation from a stronger fuel, keeping the entropy production constant, as seen in Fig. 5.

Increasing the fuel strength further, the droplet transitions from an active droplet to an excitable droplet, where the steady state is stable. Upon further increasing the fuel strength δ, cycles of formation and dissolution emerge. The transition from stationary, excitable droplets to oscillations creates a discontinuous jump in the entropy production rate $\dot{S}$ over a cycle,

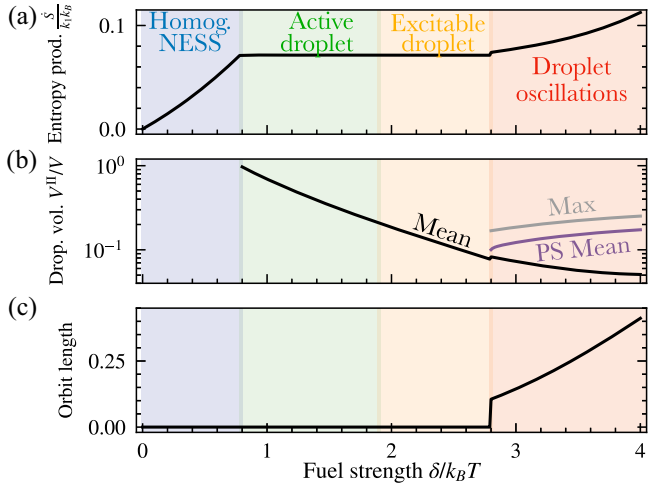

FIG. 5. Discontinuous entropy production at the onset of oscillations. Upon increasing the fuel strength δ, homogeneous NESS transits to the active droplet state with a stationary droplet volume with a kink in the entropy production $\dot{S}$. Increasing δ further decreases the droplet volume (b) but keeps the entropy production (a) constant. At the onset of formation-dissolution cycles, the entropy production $\dot{S}$ jumps [transition between the green and yellow domain in (a)]. The volume averaged over a period jumps slightly, while the peak of the wave (Max) and its mean volume when phase separated (PS Mean) [see Fig. 4(b)] show a significant jump, as well as (c) the orbit length $\int_0^\tau |\mathrm{d}\vec{\phi}|$, suggesting both as ideal readouts in experiments of self-sustained cycles.

$$\langle \dot{S} \rangle = \frac{\Omega}{2\pi} \int_0^{2\pi/\Omega} \dot{S}\, \mathrm{d}t. \tag{B5}$$

which continues to grow with fuel strength δ. As the entropy production rate jumps, so does the average droplet volume; see Fig. 5(b). An even larger jump occurs when comparing the average droplet volume when phase-separated (PS mean) and the maximum droplet volume over a cycle (Max). Formation-dissolution cycles thus permit a discontinuous increase in entropy production and larger droplet volumes as the system is driven away from equilibrium.

Appendix C: Derivation of the critical fuel strength δ^*—Here, we derive an approximate expression for the critical fuel strength δ^*, above which bistability occurs for an active droplet. To this end, we use the expression for the volume of the dense phase V^{II} at the phase-separated nullcline given in Eq. (10), and insert it into the definition of the phase-averaged total volume fraction $\bar{\psi}$ using Eq. (6). Finding the conditions for bistability is equivalent to finding nonequilibrium steady states with $\bar{\psi} < \psi_0^{\mathrm{I}}$, where $\psi_0^{\mathrm{I}} = (\phi_A^0 + \phi_B^0)/2$ is the total volume fraction where the dilute branch of the binodal intersects the nullcline of r_1 [Eq. (2)]. Solving for δ^* gives an expression the critical fuel strength necessary for bistability as a function of $\Delta\psi = \bar{\psi} - \psi^{\mathrm{I}}$,

$$e^{\frac{\delta^*}{k_BT}} = 1 + \left(1 - e^{\frac{-\Delta\mu}{k_BT}}\right)\left(\frac{k_1^{\mathrm{I}}}{k_1^{\mathrm{II}}}\left(1 + \frac{\psi^{\mathrm{II}} - \psi^{\mathrm{I}}}{\Delta\psi}\right) - 1\right), \tag{C1}$$

where $\Delta\mu = \mu_A - \mu_B$ is the chemical potential difference between A and B. As the fuel converts A to B, the chemical potential difference is negative; $\Delta\mu < 0$. So far, no approximations have been made.

Due to the nonlinearity of Eq. (C1), we perform a Taylor expansion at the point where the r_1 nullcline intersects the dilute branch of the binodal, which we denote (ϕ_A^0, ϕ_B^0). We investigate small deviations around this point, i.e., close to chemical equilibrium where $|\Delta\mu| \ll k_BT$, ignoring $\mathcal{O}(\Delta\mu/k_BT)^3$. Furthermore, we follow Ref. [37] and approximate the tie-lines to be orthogonal to the binodal. This implies that $(\psi^{\mathrm{II}} - \psi^{\mathrm{I}})$ is a constant along the binodal and can be set equal to the difference at the chemical equilibrium tie-line $(\psi_0^{\mathrm{II}} - \psi_0^{\mathrm{I}})$. We continue by introducing the angle α of the dilute branch of the binodal at (ϕ_A^0, ϕ_B^0), relative to the conserved line of $\psi_0^{\mathrm{I}} = (\phi_A^0 + \phi_B^0)/2$ at the same point, defined through $\alpha = \arctan\left((\phi_B^0 + \Delta\phi_B^{\mathrm{I}})/(\phi_A^0 + \Delta\phi_A^{\mathrm{I}})\right]$, where the $\Delta\phi_i^{\mathrm{I}}$ is the infinitesimal change in composition along the dilute branch of the binodal. This definition of the angle is such that the dilute branch of the binodal is linearized as $(\phi_A^0 - \epsilon\sin(\alpha + \pi/4), \phi_B^0 - \epsilon\sin(\alpha - \pi/4))$, where $\epsilon \simeq \Delta\psi/(\sqrt{2}\sin(\alpha))$, making $\alpha = 0$ give a dilute branch parallel to the conserved line of constant ψ. Performing this Taylor expansion in the chemical potential difference, we find $\Delta\mu \approx \Delta\psi\theta$, where

$$\theta = \frac{\cos\alpha(\phi_A^0)^{-1} + \sin\alpha(\phi_B^0)^{-1}}{\sqrt{2}\sin\alpha} + \frac{\chi_{BC} - \chi_{AC}}{k_BT} + \frac{1}{\tan\alpha}\frac{\chi_{AB}}{k_BT}. \tag{C2}$$

Using the Taylor expanded Eq. (C1), we find

$$\exp\left\{\frac{\delta^*}{k_BT}\right\} = 1 + \frac{k_1^{\mathrm{I}}}{k_1^{\mathrm{II}}}\theta(\psi_0^{\mathrm{II}} - \psi_0^{\mathrm{I}}) + (\bar{\psi} - \psi^{\mathrm{I}})\theta\left(1 - \frac{k_1^{\mathrm{I}}}{k_1^{\mathrm{II}}}(1 + \theta(\psi_0^{\mathrm{II}} - \psi_0^{\mathrm{I}}))\right). \tag{C3}$$

For the case studied, where $k_1^{\mathrm{I}} = k_1^{\mathrm{II}}$, we find the expression in Eq. (11), where we have defined

$$\Theta = \theta(\psi_0^{\mathrm{II}} - \psi_0^{\mathrm{I}}). \tag{C4}$$

Notably, the expression diverges at an angle $\alpha = 0$, and any angle $\alpha < 0$ gives a large negative value of Θ, which does not yield physical solutions of δ^* in Eq. (11). This can be understood geometrically, as the r_1 nullcline has to lie within

the binodal for multiple intersections with ψ to occur, and therefore, ψ has to also lie within the binodal. Note that α is in general negative when $\chi_{AC} > \chi_{BC}$, and positive when $\chi_{AC} < \chi_{BC}$, making the latter a necessity for bistability. The minimal value of Θ, which occurs for $\alpha = \pi/2$, is finite. Consequently, the critical fuel strength δ^* never approaches zero, and a finite fuel strength is always necessary for bistability. Note further that large values of α, which lowers the critical fuel strength, occurs when $\chi_{BC} \gg \chi_{AC}$, thereby increasing the constant offset of Θ. The predicted critical fuel strength is compared with the analytic expression in Fig. 2(e).